Enhanced Lattice QCD Studies on ε_K and ΔM_K

Yi-Kai Huo,[a,*] **Norman Christ**[a] **and Bigeng Wang**[b]

[a]*Physics Department, Columbia University,*
New York, NY 10027, USA

[b]*Department of Physics and Astronomy, University of Kentucky,*
Lexington, KY 40506, USA

E-mail: yh3285@columbia.edu, nhc@phys.columbia.edu, bwa271@g.uky.edu

Two second-order quantities related to K meson mixing, ε_K and ΔM_K, are Standard Model observables that are highly sensitive to possible new physics. The RBC and UKQCD collaborations have presented results for ΔM_K with physical quark masses and the first lattice calculation of the long-distance part of ε_K. Utilizing new-generation computers and new lattice configurations with an inverse lattice spacing of 2.7 GeV and physical quark masses, we can extend this previous work to obtain more precise results.

The 41st International Symposium on Lattice Field Theory (LATTICE2024)
28 July - 3 August 2024
Liverpool, UK

*Speaker

1. Introduction

The weak interaction sector of the Standard Model remains the least understood among its components. The weak interaction naturally enables the violation of parity symmetry and charge-parity (CP) symmetry. Its interplay with strong interaction processes, contributes to the intricate nature of flavor symmetry. These symmetry-violating processes provide intriguing opportunities to test the validity of the Standard Model, as any deviation from its predictions could signal the existence of new physics. Among such tests, the $K^0 - \bar{K}^0$ system is particularly compelling, as the kaon is the lightest meson containing a strange quark. This mixing is a second-order weak interaction process mediated by the exchange of two W bosons. The CP-conserved component of this system corresponds to the mass difference between the long- and short-lived kaon states (ΔM_K), while the CP-violating component is characterized by ε_K. Both parameters have been experimentally observed, making this system a valuable tool for probing the Standard Model.

The experimental value of ΔM_K is $3.483(6) \times 10^{-12}$ MeV. Previous perturbative calculations of ΔM_K treat the charm quark perturbatively, leading to a local $\Delta S = 2$ operator corresponding to the kaon bag parameter. However, for this process the perturbative expansion appears to converge very slowly: the NNLO contribution is as large as 36% of the sum of LO and NLO contributions [1]. This slow convergence highlights the potential benefits of performing a non-perturbative calculation using lattice QCD. The RBC-UKQCD collaboration has obtained a ΔM_K result using physical quark masses and a lattice spacing corresponding to $1/a = 2.36$ GeV [2]. However, an improved calculation is necessary on a physically larger and finer lattice to achieve better control over finite volume effects and discretization errors and to enable a more reliable continuum-limit extrapolation. Additionally, a more accurate treatment of the two-pion intermediate state is required to further refine the results.

The mixing parameter ε_K characterizes indirect CP violation and has an experimental value of $2.228(11) \times 10^{-3}$. The perturbative calculation of the short-distance contribution to ε_K has been highly successful, contributing the majority of the total result [1, 3]. However, a small but significant portion, comprising a few percent, arises from the long-distance contributions. A first-principles non-perturbative calculation is therefore a natural choice to address this gap. The RBC-UKQCD collaboration has performed the first calculation of the long-distance part of ε_K using a light quark mass corresponding to a pion mass 339 MeV and a charm quark mass 968 MeV [4]. We plan to calculate ΔM_K and ε_K on lattice ensembles with physical quark masses to obtain physical results with better controlled systematic errors and improved statistics.

2. Kaon Mixing

K^0 and $\bar{K}^0$ mesons are eigenstates of the strong interaction: the K^0 has strangeness $+1$ and the $\bar{K}^0$ has strangeness -1. The Wigner-Weisskopf theory describes the time evolution of neutral kaon system [5]:

$$i\frac{d}{dt}\begin{pmatrix} |K^0(t)\rangle \\ |\bar{K}^0(t)\rangle \end{pmatrix} = \left(\begin{pmatrix} M & M_{0\bar{0}} \\ M_{0\bar{0}}^* & M \end{pmatrix} - \frac{i}{2}\begin{pmatrix} \Gamma & \Gamma_{0\bar{0}} \\ \Gamma_{0\bar{0}}^* & \Gamma \end{pmatrix} \right)\begin{pmatrix} |K^0(0)\rangle \\ |\bar{K}^0(0)\rangle \end{pmatrix}, \tag{1}$$

To preserve CPT symmetry, the diagonal elements must be identical, and the off-diagonal elements of M and Γ are required to satisfy the condition of hermiticity. Experimental results have shown

that CP violation in the neutral kaon system is very weak: the imaginary parts of the off-diagonal elements are much smaller than their real parts. Consequently, ΔM_K can be approximated as the real part of the dispersive off-diagonal term $M_{0\bar{0}}$:

$$\Delta M_K = M_L - M_S = 2\text{Re}Q \simeq 2\text{Re}M_{0\bar{0}} \tag{2}$$

The parameter ε_K is related to the ratio of the imaginary part to the real part of $M_{0\bar{0}}$ as follows:

$$\varepsilon_K = e^{i\phi_\varepsilon} \sin\phi_\varepsilon \left(\frac{-\text{Im}\,M_{\bar{0}0}}{\Delta M_K} + \frac{\text{Im}\,A_0}{\text{Re}\,A_0} \right), \tag{3}$$

where A_0 represents the amplitude of the $K \to \pi\pi$ decay with isospin 0, and the angle ϕ_ε is defined as:

$$\phi_\varepsilon = \tan^{-1}\left(\frac{2\Delta M_K}{\Gamma_S - \Gamma_L} \right) = 43.51(5)^\circ. \tag{4}$$

3. Lattice Calculation of ΔM_K

The Glashow–Iliopoulos–Maiani(GIM) mechanism indicates the dominant contribution to ΔM_K arises from energy scales around or below the charm quark mass. By selecting an energy scale μ larger than the charm quark mass, one can effectively separate the long-distance and short-distance contributions to ΔM_K. The long-distance contribution is calculated using lattice QCD and involves the bi-local product of two $\Delta S = 1$ effective Hamiltonian operators, between which the active charm quark can propagate. There is also a short-distance contribution to this long-distance part that is incorporated through Wilson coefficients, which are determined by integrating out the weak interaction and QCD effects at a sufficiently high energy scale. Consequently, ΔM_K can be expressed as:

$$\Delta M_K = 2\mathcal{P} \sum_n \frac{\langle \bar{K}^0 | H_W^{\Delta S=1} | n \rangle \langle n | H_W^{\Delta S=1} | K^0 \rangle}{M_K - E_n}, \tag{5}$$

where $H_W^{\Delta S=1}$ denotes the $\Delta S = 1$ effective Hamiltonian operator, defined as:

$$H_W^{\Delta S=1} = \frac{G_F}{\sqrt{2}} \sum_{q,q'=u,c} V_{q's}^* V_{qd} \left(C_1 Q_1^{q'\bar{q}} + C_1 Q_2^{q'\bar{q}} \right), \tag{6}$$

where $Q_1^{qq'}$ and $Q_2^{qq'}$ are current-current operators, defined as:

$$Q_1^{q'\bar{q}} = (\bar{s}_a q_b')_{V-A}(\bar{q}_b d_a)_{V-A}, \quad Q_2^{q'\bar{q}} = (\bar{s}_a q_a')_{V-A}(\bar{q}_b d_b)_{V-A}, \tag{7}$$

where $V - A$ denotes a left-handed vertex and the Roman indices a and b label color components. A more detailed setup has been discussed in [6, 7].

One can extract ΔM_K through a single integration of the four-point correlation functions computed using lattice QCD over the time t_2, as illustrated in Fig. 1:

$$\mathcal{A}^S(T,t_1) = \frac{1}{2!} \sum_{t_2=t_1-T}^{t_1+T} \langle 0 | T\{\bar{K}^0(t_f) H_W(t_2) H_W(t_1) K^0(t_i)\} | 0 \rangle$$

$$= N_K^2 e^{-M_K(t_f - t_i)} \left\{ \sum_n \frac{\langle \bar{K}^0 | H_W | n \rangle \langle n | H_W | K^0 \rangle}{M_K - E_n} \left(-1 + e^{(M_K - E_n)(T+\frac{1}{2})} \right) \right\}, \tag{8}$$

where the red-highlighted term represents our target. A further average over the time t_1 will improve the statistics.

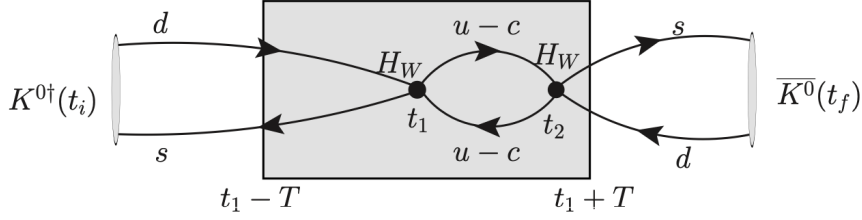**Figure 1:** Example of bi-local structure calculated on lattice

4. Lattice Calculation of ε_K

Since ε_K is a CP-violating parameter, the contribution from the top quark is no longer suppressed, and the GIM mechanism ceases to be relevant. Consequently, the short-distance contribution becomes dominant. In this case, $M_{0\bar{0}}$ can be expressed as the $K^0 - \bar{K}^0$ matrix element of a local $\Delta S = 2$ effective Hamiltonian operator, $H_W^{\Delta S=2}$.

For convenience in implementing our lattice calculation, we adopt a charm-quark subtraction scheme, where the unitarity condition is used to eliminate the factor λ_c, rather than an up-quark subtraction scheme, which eliminates λ_u, where $\lambda_q = V_{qd}^* V_{qs}$ for $q = u$, c or t. This choice reduces the number of amplitudes that need to be computed using lattice QCD. The modified effective Hamiltonian can be written as follows:

$$H_W^{\Delta S=2} = \frac{G_F^2}{16\pi^2} M_W^2 \left[\lambda_u^2 \eta_1' S_0'(x_c) + \lambda_t^2 \eta_2' S_0'(x_t) + 2\lambda_u\lambda_t \eta_3' S_0'(x_t, x_c) \right] O_{LL} + \text{h.c.}, \tag{9}$$

where

$$O_{LL} = \bar{s}\gamma_\mu(1-\gamma_5)d\,\bar{s}\gamma_\mu(1-\gamma_5)d. \tag{10}$$

In Eq. 9, the λ_u^2 term is purely real and constitutes the primary contribution to ΔM_K. The λ_t^2 term can be computed perturbatively due to the heavy mass of the top quark. The $\lambda_u\lambda_t$ term is the only component that requires a long-distance calculation using lattice QCD. Hence, starting from the $\Delta S = 1$ Hamiltonian $H_W^{\Delta S=1}$, an explicit effective Hamiltonian can be derived, which is distinctly separated into $\lambda_u\lambda_t$ terms and other contributions, facilitating our lattice calculation [9].

$$H_W^{\Delta S=1} = \frac{G_F}{\sqrt{2}} \left(\sum_{q,q'=u,c} V_{q's}^* V_{qd} \sum_{i=1,2} C_i Q_i^{q'\bar{q}} - \lambda_t \sum_{i=3}^{6} C_i Q_i \right) \tag{11}$$

where $Q_1^{qq'}$ and $Q_2^{qq'}$ are current-current operators and $Q_i, 3 \le i \le 6$ are QCD penguin operators:

$$
\begin{aligned}
Q_1^{q'\bar{q}} &= (\bar{s}_a q_b')_{V-A}(\bar{q}_b d_a)_{V-A}, & Q_2^{q'\bar{q}} &= (\bar{s}_a q_a')_{V-A}(\bar{q}_b d_b)_{V-A}, \\
Q_3 &= (\bar{s}_a d_a)_{V-A} \sum_{q=u,d,s,c} (\bar{q}_b q_b)_{V-A}, & Q_4 &= (\bar{s}_a d_b)_{V-A} \sum_{q=u,d,s,c} (\bar{q}_b q_a)_{V-A}, \\
Q_5 &= (\bar{s}_a d_a)_{V-A} \sum_{q=u,d,s,c} (\bar{q}_b q_b)_{V+A}, & Q_6 &= (\bar{s}_a d_b)_{V-A} \sum_{q=u,d,s,c} (\bar{q}_b q_a)_{V+A}.
\end{aligned}
\tag{12}
$$

4

The current-current operators involve all combinations of up and charm quarks, $q'\bar{q}$. The QCD penguin operators, on the other hand, are summed over all four quark flavors. Here, $V - A$ denotes a left-handed vertex, while $V + A$ denotes a right-handed vertex and the Roman indices a and b label color components.

The $\lambda_u\lambda_t$ terms receive contributions from two types of bi-local structures. The first comes from cases where both operators are current-current operators, while the second arises from combinations of a current-current operator and a QCD penguin operator. The resulting explicit effective operator can be expressed as follows:

$$H_{\text{eff},ut}^{\Delta S=2} = \frac{G_F^2}{2}\lambda_u\lambda_t \sum_{i=1,2}\left\{\sum_{j=1}^{6}C_iC_j\sum_{x,y}\left[\left[\widetilde{Q}_i\widetilde{Q}_j(x,y)\right]\right] + C_{7i}\sum_x O_{LL}(x)\right\}, \quad (13)$$

$$\left[\left[\widetilde{Q}_i\widetilde{Q}_j(x,y)\right]\right] = \frac{1}{2}T\{Q_i^{c\bar{c}}(x)(Q_j^{c\bar{c}}(y) - Q_j^{u\bar{u}}(y)) + (Q_i^{c\bar{c}}(x) - Q_i^{u\bar{u}}(x))Q_j^{c\bar{c}}(y)$$
$$- Q_i^{u\bar{c}}(x)Q_j^{c\bar{u}}(y) - Q_i^{c\bar{u}}(x)Q_j^{u\bar{c}}(y)\}, \quad (i,j = 1,2), \quad (14)$$

$$\left[\left[\widetilde{Q}_i\widetilde{Q}_j(x,y)\right]\right] = \frac{1}{2}T\left\{\left[Q_i^{c\bar{c}}(x) - Q_i^{u\bar{u}}(x)\right]Q_j(y)\right.$$
$$\left. + Q_j(x)\left[Q_i^{c\bar{c}}(y) - Q_i^{u\bar{u}}(y)\right]\right\}, \quad (i = 1,2; j = 3,...,6). \quad (15)$$

$\left[\left[\widetilde{Q}_i\widetilde{Q}_j(x,y)\right]\right]$ describes the long-distance corrections, which we aim to determine through lattice QCD calculations. A more detailed setup has been discussed in [4].

5. Short-Distance Divergence and Renormalization

The GIM mechanism and the $V-A$ structure effectively eliminate both quadratic and logarithmic divergences in ΔM_K as can be seen from the one loop integral resulting from the charm and up quark contractions without QCD corrections:

$$\int d^4p\,\gamma^\mu(1-\gamma^5)\left(\frac{\not{p}-m_c}{p^2+m_c^2} - \frac{\not{p}-m_u}{p^2+m_u^2}\right)\gamma^\nu(1-\gamma^5)\left(\frac{\not{p}-m_c}{p^2+m_c^2} - \frac{\not{p}-m_u}{p^2+m_u^2}\right)$$
$$= \int d^4p\,\gamma^\mu(1-\gamma^5)\frac{\not{p}(m_u^2-m_c^2)}{(p^2+m_u^2)(p^2+m_c^2)}\gamma^\nu(1-\gamma^5)\frac{\not{p}(m_u^2-m_c^2)}{(p^2+m_u^2)(p^2+m_c^2)}. \quad (16)$$

However, with reduced protection from the GIM mechanism and the inclusion of penguin operators, the calculation of the product of the bi-local structure encounters a logarithmic divergence when the two operators coincide:

$$\int d^4p\,\gamma^\mu(1-\gamma^5)\left(\frac{\not{p}-m_c}{p^2+m_c^2} - \frac{\not{p}-m_u}{p^2+m_u^2}\right)\gamma^\nu(1-\gamma^5)\left(\frac{\not{p}-m_c}{p^2+m_c^2}\right)$$
$$= \int d^4p\,\gamma^\mu(1-\gamma^5)\frac{\not{p}(m_u^2-m_c^2)}{(p^2+m_u^2)(p^2+m_c^2)}\gamma^\nu(1-\gamma^5)\frac{\not{p}}{p^2+m_c^2}. \quad (17)$$

This short-distance divergence can be removed by adding a counterterm, which is the product of a coefficient and the local operator O_{LL}. The explicit form of this counterterm has been defined in the $\overline{\text{MS}}$ scheme [9]. In lattice calculations, the short-distance correction is typically implemented using the regularization-independent (RI/SMOM) method [10–12]. At a given scale μ_{RI}, the RI/SMOM

renormalization condition requires that the product of the local operator O_{LL} and coefficients X_{ij}^{Lat} cancels the bi-local operators in a Landau-gauge-fixed Green's function with four external quark lines, where the off-shell momenta (p_1, p_2, p_3, p_4) are specified at the scale μ_{RI}:

$$\left(\Gamma_{\alpha\beta\gamma\delta,ij}^{\text{bilocal,amp}}(p_1, p_2, p_3, p_4) - X_{ij}^{\text{Lat}}(\mu_{\text{RI}})\Gamma_{\alpha\beta\gamma\delta}^{\text{local,amp}}(p_1, p_2, p_3, p_4)\right) P_{\alpha\beta\gamma\delta} = 0. \tag{18}$$

$\Gamma_{\alpha\beta\gamma\delta,ij}^{\text{bilocal,amp}}$ and $\Gamma_{\alpha\beta\gamma\delta,ij}^{\text{local,amp}}$ represent the amputated Green's functions corresponding to the bi-local and local operators, respectively. Since the Green's function is constrained to vanish at specific momenta under the RI/SMOM condition, it is necessary to restore its appropriate value by connecting the regularization-independent scheme to the $\overline{\text{MS}}$ scheme. To achieve this, a coefficient $Y_{ij}^{\overline{\text{MS}}}(\mu_{\overline{\text{MS}}}, \mu_{\text{RI}})$ is introduced to apply the required correction:

$$\int d^4x [[\widetilde{Q}_i^{\overline{\text{MS}}}(x)\widetilde{Q}_j^{\overline{\text{MS}}}(0)]]^{\overline{\text{MS}}} \;\;=\;\; \int d^4x [[\widetilde{Q}_i^{\overline{\text{MS}}}(x)\widetilde{Q}_j^{\overline{\text{MS}}}(0)]]^{\text{RI}} + Y_{ij}^{\overline{\text{MS}}}(\mu_{\overline{\text{MS}}}, \mu_{\text{RI}})O_{LL.}^{\overline{\text{MS}}} \tag{19}$$

The final form of the matrix elements calculated on the lattice is expressed as follows:

$$\begin{aligned}
\mathcal{H}_{W,ut}^{\Delta S=2} \;\;=\;\; & \frac{G_F^2}{2}\lambda_u\lambda_t \sum_{i=1}^{2}\left\{\sum_{j=1}^{6} C_i^{\text{Lat}}C_j^{\text{Lat}}\left(\sum_x [[\widetilde{Q}_i^{\text{Lat}}(x)\widetilde{Q}_j^{\text{Lat}}(0)]]^{\text{Lat}} - X_{ij}^{\text{Lat}}(\mu_{\text{RI}})O_{LL}^{\text{Lat}}(0)\right)\right. \\
& \left. + \left(C_{7i}^{\overline{\text{MS}}} + \sum_{j=1}^{6} C_i^{\overline{\text{MS}}}C_j^{\overline{\text{MS}}}Y_{ij}^{\overline{\text{MS}}}(\mu_{\overline{\text{MS}}}, \mu_{\text{RI}})\right)Z_{LL}^{\text{Lat}\to\overline{\text{MS}}}O_{LL}^{\text{Lat}}(0)\right\}.
\end{aligned} \tag{20}$$

The first line in Eq. 20 eliminates the divergence from the lattice calculation by applying the RI/SMOM condition. The second line represents the counterterm defined in the $\overline{\text{MS}}$ scheme, along with the matching term that connects the $\overline{\text{MS}}$ scheme to the RI/SMOM scheme.

However, due to the lack of precise perturbative results for the correction coefficient $Y_{ij}^{\overline{\text{MS}}}(\mu_{\overline{\text{MS}}}, \mu_{\text{RI}})$ at a non-zero energy scale μ_{RI}, we rely on the NNLO result for $Y_{ij}^{\overline{\text{MS}}}(\mu_{\overline{\text{MS}}}, 0)$ [3, 13]. In previous work by our collaboration, a rough leading-order (LO) matching term $\Delta Y_{ij}^{\overline{\text{MS}}}(\mu_{\overline{\text{MS}}}, \mu_{\text{RI}})$ at order α_s^0 was introduced to address this limitation:

$$\Delta Y_{ij}^{\overline{\text{MS}}}(\mu_{\overline{\text{MS}}}, \mu_{\text{RI}}) = Y_{ij}^{\overline{\text{MS}}}(\mu_{\overline{\text{MS}}}, \mu_{\text{RI}}) - Y_{ij}^{\overline{\text{MS}}}(\mu_{\overline{\text{MS}}}, 0). \tag{21}$$

This incomplete calculation reduces the accuracy of the final results, highlighting the need for a higher-order perturbative RI/SMOM to $\overline{\text{MS}}$ matching calculation.

6. Numerical Setup

We will perform our enhanced lattice calculations of ΔM_K and ε_K using two sets of configurations with physical quark masses, as summarized in Table 1. To complete this calculation, we have a significant allocation on Frontier, the leadership class computer at the Oak Ridge National Laboratory. Frontier has 9,408 AMD compute nodes in total. Each node contains one 64-core AMD CPU (with 2 hardware threads per physical core) with access to 512 GB of DDR4 memory and 4 AMD cards, each with 2 Graphics Compute Dies (GCDs) for a total of 8 GCDs(logically equivalent to 8 separate GPUs). An additional powerful enhancement is our computing software

Name	Action	a^{-1}(GeV)	Volume	m_π(MeV)	Size(fm)
64I	MDWF+I	2.359(7)	$64^3 \times 128 \times 12$	139	5.4
96I	MDWF+I	2.708	$96^3 \times 192 \times 12$	140	6.9

Table 1: Dynamical 2+1 flavor domain wall fermion lattices to be used in our calculation, MDWF = Mobius domain wall fermions, I = Iwasaki gauge action.

architecture, Grid [8, 14, 15]. Grid is a high-performance C++ library designed to geometrically decompose lattice calculations into MPI tasks while also leveraging SIMD lanes. The local vector loops are parallelized using OpenMP pragmas. Grid supports heterogeneous computing architectures, enabling it to maximize the computational potential of GPUs for matrix operations. With this state-of-the-art hardware and advanced software infrastructure, we can achieve exceptional computational capabilities to carry out our lattice calculations efficiently and effectively. To enhance the efficiency of propagator solving, we have implemented the following strategies:

- **Utilizing Eigenvectors of the Dirac Operator**
  We leverage the eigenvectors of the Dirac operator, generated via the Lanczos algorithm, to accelerate the computation. These eigenvectors are used to construct a preconditioner. This preconditioner significantly reduces the number of conjugate gradient iterations required for propagator solving by lowering the condition number of the Dirac matrix, thus making the overall solving process more efficient and stable. [16]

- **Mixed-Precision Inversion**
  A mixed-precision approach is applied during the inversion process to balance performance and accuracy. In each outer iteration, we first invert using the residual vectors as sources in single precision, which allows for faster computations and provides a reasonably good initial estimate. Then we perform a double-precision correction step to ensure the desired accuracy of the final solution. This method significantly reduces computation time while maintaining high precision in the results.

- **Incorporating BLAS in the Lanczos Preconditioner**
  To further optimize massive inner-product operations in the Lanczos preconditioner, we exploited the Grid support for BLAS (Basic Linear Algebra Subprograms), specifically the batched version of GEMM (matrix-matrix multiplication). By utilizing GemmBatch, the batched operation efficiently processes multiple independent dot products in parallel, leveraging GPU resources to minimize idle time and maximize computational throughput. Consequently, we significantly accelerate the process of projecting a vector onto eigenvectors, especially when handling a large number of eigenvectors. [17]

7. Conclusion

In combination with the previous calculations, as outlined in Table 1, we can compute ΔM_K and long-distance contribution to ε_K using data from two distinct lattice spacings. This will enable

us to perform an extrapolation to the continuum limit, ensuring more accurate and reliable results in the near future. What's more, we are hoping to exploit a new RBC/UKQCD ensemble whose generation was begun very recently. This ensemble has a lattice volume of $128^3 \times 288$ and an inverse lattice spacing of 3.5 GeV. When available, this ensemble will allow even greater precision for calculations such as those described here in which a propagating charm quark plays an important role.

Acknowledgments

References

[1] J. Brod and M. Gorbahn, *Next-to-Next-to-Leading-Order Charm-Quark Contribution to the CP Violation Parameter ε_K and ΔM_K*, *Phys. Rev. Lett.* **108** (2012) 121801 [1108.2036].

[2] B. Wang, *Calculating Δm_K with lattice QCD*, *PoS* **LATTICE2021** (2022) 141 [2301.01387].

[3] J. Brod and M. Gorbahn, *ε_K at Next-to-Next-to-Leading Order: The Charm-Top-Quark Contribution*, *Phys. Rev. D* **82** (2010) 094026 [1007.0684].

[4] Z. Bai, N. H. Christ, J. M. Karpie, C. T. Sachrajda, A. Soni and B. Wang, *Long-distance contribution to ε_K from lattice QCD*, *Phys. Rev. D* **109** (2024) 054501 [2309.01193].

[5] A. Pich, *CP violation*, *ICTP Ser. Theor. Phys.* **10** (1994) 14 [hep-ph/9312297].

[6] N. H. Christ *et al.* [RBC and UKQCD], *Long distance contribution to the KL-KS mass difference*, *Phys. Rev. D* **88** (2013) 014508 [1212.5931].

[7] B. Wang, *Lattice calculation of the mass difference between the long- and short-lived K mesons for physical quark masses*, PhD thesis, Columbia University (2021)

[8] P. Boyle, A. Yamaguchi, G. Cossu and A. Portelli, *Grid: A next generation data parallel C++ QCD library*, 1512.03487.

[9] G. Buchalla, A. J. Buras and M. E. Lautenbacher, *Weak decays beyond leading logarithms*, *Rev. Mod. Phys.* **68** (1996) 1125 [hep-ph/9512380].

[10] C. Sturm, Y. Aoki, N. H. Christ, T. Izubuchi, C. T. C. Sachrajda and A. Soni, *Renormalization of quark bilinear operators in a momentum-subtraction scheme with a nonexceptional subtraction point*, *Phys. Rev. D* **80** (2009) 014501 [0901.2599].

[11] G. Martinelli, C. Pittori, C. T. Sachrajda, M. Testa and A. Vladikas, *A General method for nonperturbative renormalization of lattice operators*, *Nucl. Phys. B* **445** (1995) 81 [hep-lat/9411010].

[12] Y. Aoki, P. A. Boyle, N. H. Christ, C. Dawson, M. A. Donnellan, T. Izubuchi, A. Juttner, S. Li, R. D. Mawhinney and J. Noaki, *et al. Non-perturbative renormalization of quark bilinear operators and B(K) using domain wall fermions*, *Phys. Rev. D* **78** (2008) 054510 [0712.1061].

[13] J. A. Bailey *et al.* [SWME], *Current status of ε_K with lattice QCD inputs*, *PoS* **CORFU2022** (2023) 028 [1503.06613].

[14] A. Yamaguchi, P. Boyle, G. Cossu, G. Filaci, C. Lehner and A. Portelli, *Grid: OneCode and FourAPIs*, *PoS* **LATTICE2021** (2022) 035 [2203.06777].

[15] P. A. Boyle. *Grid: A C++ mathematical object library for lattice field theory simulations*, GitHub repository (2025).

[16] M. Luscher, *Deflation acceleration of lattice QCD simulations*, *JHEP* **12** (2007) 011 [0710.5417].

[17] P. A. Boyle, *Multiple right hand side multigrid for domain wall fermions with a multigrid preconditioned block conjugate gradient algorithm*, 2409.03904.